Closed headpiece of integrin $\alpha_{IIb}\beta_3$ and its complex with an $\alpha_{IIb}\beta_3$-specific antagonist that does not induce opening

*Jieqing Zhu,[1] *Jianghai Zhu,[1] *Ana Negri,[2] Davide Provasi,[2] Marta Filizola,[2] Barry S. Coller,[3] and Timothy A. Springer[1]

[1]Immune Disease Institute, Children's Hospital Boston, and Department of Pathology, Harvard Medical School, Boston, MA; [2]Department of Structural and Chemical Biology, Mount Sinai School of Medicine, New York, NY; and [3]Laboratory of Blood and Vascular Biology, Rockefeller University, New York, NY

The platelet integrin $\alpha_{IIb}\beta_3$ is essential for hemostasis and thrombosis through its binding of adhesive plasma proteins. We have determined crystal structures of the $\alpha_{IIb}\beta_3$ headpiece in the absence of ligand and after soaking in RUC-1, a novel small molecule antagonist. In the absence of ligand, the $\alpha_{IIb}\beta_3$ headpiece is in a closed conformation, distinct from the open conformation visualized in presence of Arg-Gly-Asp (RGD) antagonists. In contrast to RGD antagonists, RUC-1 binds only to the α_{IIb} subunit. Molecular dynamics revealed nearly identical binding. Two species-specific residues, α_{IIb} Y190 and α_{IIb} D232, in the RUC-1 binding site were confirmed as important by mutagenesis. In sharp contrast to RGD-based antagonists, RUC-1 did not induce $\alpha_{IIb}\beta_3$ to adopt an open conformation, as determined by gel filtration and dynamic light scattering. These studies provide insights into the factors that regulate integrin headpiece opening, and demonstrate the molecular basis for a novel mechanism of integrin antagonism. (*Blood*. 2010;116(23):5050-5059)

Introduction

Integrins are cell surface–adhesion receptors that contain noncovalently associated α and β subunits, each with a single-pass transmembrane domain and a typically short cytoplasmic domain.[1,2] Ectodomains are structurally complex, with 4 or 5 domains in α and 8 in β. The α and β subunits come together in the integrin head to form the binding site for ligands. Crystal structures of full-length ectodomains of integrins $\alpha_V\beta_3$, $\alpha_{IIb}\beta_3$, and $\alpha_X\beta_2$ have all revealed a compact, bent conformation.[3-6] The α and β subunits are each acutely bent at their knees, between the upper- and lower-leg domains (Figure 1A). The bend brings head and upper-leg domains (collectively termed "the headpiece") into intimate contact with the lower-leg domains. An extensive, largely hydrophilic surface of > 4000 Å^2 between the headpiece and lower legs, and between the α and β legs, becomes solvent exposed on integrin extension (Figure 1A). A large body of crystallographic, electron microscopic (EM), and mutational evidence shows that the bent conformation represents the low affinity, resting state of integrins,[7] although some studies have nonetheless reached different conclusions.[3,8,9]

Two types of fundamental conformational changes have been found in integrins based on EM and crystallographic data: (1) integrin extension at the knees and (2) swing out at the interface between the β subunit βI and hybrid domains, converting the headpiece from the closed to the open conformation (Figure 1A). The C-terminal α7-helix of the βI domain links conformational changes at the interface with the hybrid domain to the opposite end of the βI domain, changing conformation and affinity at the ligand binding site at the interface with the α subunit β-propeller domain. Integrin affinity up-regulation is intimately associated with the transition from the closed to open headpiece conformation.[7]

Previously, complete ectodomain and headpiece integrin crystal structures have revealed different headpiece conformations. In the complete ectodomain crystal structures, integrin headpieces adopt a closed conformation.[3-6] Before the current study, the only crystal structures of an integrin headpiece fragment, those of $\alpha_{IIb}\beta_3$, were found in open conformation. All of these structures contained an $\alpha_{IIb}\beta_3$ ligand, ligand mimetic, or pseudoligand that coordinated the metal ion–dependent adhesion site (MIDAS) Mg^{2+}, supporting the hypothesis that ligand binding induces and/or stabilizes the open/swung-out conformation.[10,11] The possibility has been raised, however, that the open headpiece conformation was not the result of ligand binding, but rather a loss of the lower legs and associated headpiece-tailpiece interactions.[12] We considered this hypothesis unlikely, however, because ligand and ligand-mimetic drugs induce the open headpiece conformation in both headpiece fragments and the entire ectodomain, as demonstrated by small angle x-ray scattering and EM.[1,7,13-16] In fact, EM studies show that when the entire integrin ectodomain extends, individual molecules can have either a closed or open headpiece.[15,17] Nonetheless, a crystal structure of a headpiece fragment in closed conformation would exclude the possibility that the open conformation was an artifact of truncation. Furthermore, because the hybrid domain has extensive contacts with lower-leg domains in the bent conformation[4-6] (Figure 1A), in the absence of such restraints in a headpiece fragment, it would be interesting to know if atomic details at the ligand binding site and the βI/hybrid domain interface would differ from those seen in the bent conformation. Moreover, if such a closed conformation lacked a ligand or pseudoligand, it would further add to the correlation between ligand binding and headpiece opening. In addition, because controversy remains as to whether integrins bind metal ions before or after ligand binding,[5,6,18] the occupancy of metal binding sites would also be of interest.

Submitted April 20, 2010; accepted July 26, 2010. Prepublished online as *Blood* First Edition paper, August 2, 2010; DOI 10.1182/blood-2010-04-281154.

*Jieqing Zhu, Jianghai Zhu, and Ana Negri contributed equally to this paper.

The online version of this article contains a data supplement.

The publication costs of this article were defrayed in part by page charge payment. Therefore, and solely to indicate this fact, this article is hereby marked "advertisement" in accordance with 18 USC section 1734.

Highly expressed on platelets, integrin $\alpha_{IIb}\beta_3$ plays an essential role in the maintenance of hemostasis and the formation of pathologic platelet-mediated thrombi.[19] $\alpha_{IIb}\beta_3$ recognizes an Arg-Gly-Asp (RGD) sequence in ligands as well as the Lys-Gln-Ala-Gly-Asp-Val (KQAGDV) sequence of the fibrinogen γC module.[10,20] Two FDA-approved RGD-mimetic $\alpha_{IIb}\beta_3$ antagonists, tirofiban and eptifibatide, are currently in use for the treatment of select thrombotic complications of cardiovascular disease.[21,22] Cocrystallization of these drugs with the integrin $\alpha_{IIb}\beta_3$ headpiece revealed that they bind in the same way as peptides containing the RGD sequence.[10,11] The basic Arg side chain or nitrogen-containing drug moiety binds to Asp-224 in a pocket of the α_{IIb} β-propeller domain whereas the acidic Asp side chain or a carboxyl moiety in the drug directly coordinates the MIDAS Mg^{2+} ion in the β_3 βI domain.[11,23] Ligand binding stabilizes the open headpiece conformation, which is characterized by a coordinated series of movements, including: (1) movement of the βI domain β1-α1 loop toward the ligand, (2) movement of the β6-α7 loop "downward," and (3) piston-like movement of the α7-helix downward, causing a large swing-out movement of the hybrid domain, which is visible as the open headpiece conformation at EM and small angle x-ray scattering resolution.[14,15,17]

Conformational changes in the $\alpha_{IIb}\beta_3$ receptor on the platelet surface in patients treated with RGD-mimetics have potentially important implications for therapy.[24-31] Preexisting or neoantigen-induced drug-dependent antibodies to $\alpha_{IIb}\beta_3$ may be responsible, at least in part, for the thrombocytopenia observed in as many as 5% of treated patients.[29-31] Furthermore, a paradoxical increase in the risk of thrombosis was observed in association with treatment using some orally active, RGD-mimetic $\alpha_{IIb}\beta_3$ antagonists.[32] In some cases, autoantibodies that can bind to ligand-induced binding site (LIBS) epitopes can activate patient platelets by simultaneously engaging the platelet Fc receptor.[30] In the majority of cases, however, the etiology of thrombosis is unclear. One possible explanation is that RGD-mimetic antagonists induce the high-affinity state of the receptor, thus priming it to bind ligand after drug dissociation from the receptor.[32-34] Ligand binding could then support platelet aggregation and potentially contribute to an increase in cardiovascular events.[32-33]

A novel small molecule (M_r 265) $\alpha_{IIb}\beta_3$ antagonist termed RUC-1 is effective in inhibiting platelet aggregation in vitro as well as thrombus formation in experimental models in vivo.[35,36] RUC-1 is specific for $\alpha_{IIb}\beta_3$ relative to $\alpha_V\beta_3$. It demonstrates little or no $\alpha_{IIb}\beta_3$-priming activity and induces little or no exposure of the β_3 LIBS epitope recognized by monoclonal antibody AP5. Preliminary molecular docking studies suggested that, in contrast to RGD-mimetics, which bind to both the α_{IIb} and the β_3 subunits, RUC-1 binds exclusively to the α_{IIb} subunit.

We report the first crystal structure for an integrin headpiece fragment in the absence of a peptide ligand, ligand mimetic, or pseudoligand. Despite the absence of leg domains, the headpiece is in closed conformation. The crystal structure in the presence of RUC-1 confirmed that RUC-1 binds exclusively to α_{IIb} and provides the atomic details of its binding site. RUC-1 binding is not associated with remodeling to the high-affinity state, as further confirmed by gel filtration and dynamic light scattering (DLS). Molecular dynamics (MD) simulations and mutagenesis provide additional support for the proposed RUC-1 binding mechanism.

Methods

Protein expression, purification, and crystallography

The soluble $\alpha_{IIb}\beta_3$ headpiece construct contains residues 1-621 of α_{IIb} and 1-472 of β_3 (Figure 1B).[11] The $\alpha_{IIb}\beta_3$ headpiece was stably expressed in CHO Lec.3.2.8.1 cells and purified with a Ni-NTA column (Figure 1B). After chymotrypsin digestion and a second Ni-NTA column purification, it was further purified by gel filtration (Figure 1C). The thigh domain of the α_{IIb} subunit remained after chymotrypsin digestion based on the molecular weight (~67 kDa) deduced by sodium dodecyl sulfate–polyacrylamide gel electrophoresis (Figure 1C). This untagged $\alpha_{IIb}\beta_3$ headpiece was used for gel filtration and DLS studies, as described below. The untagged $\alpha_{IIb}\beta_3$ headpiece-10E5 Fab complex was purified by gel filtration and treated with carboxypeptidase A and B in the presence of 1mM Zn^{2+}, and purified by gel filtration in Tris-buffered saline with 1mM Ca^{2+}/Mg^{2+}. Carboxypeptidase treatment removed the α_{IIb}-thigh domain, decreasing the molecular weight to ~ 50 kDa (Figure 1D). There was no molecular weight change for the β_3 subunit after carboxypeptidase treatment (Figure 1C-D). The $\alpha_{IIb}\beta_3$/Fab complex was concentrated in Tris-buffered saline with 1mM Ca^{2+}/Mg^{2+} to 10 mg/mL and crystallized in 11% PEG 8000, 0.2M ammonium sulfate, 0.1M Tris-HCl, pH 8.9 at 4°C. RUC-1 was soaked into the $\alpha_{IIb}\beta_3$/Fab crystals at 500μM in the well solution containing 1mM Ca^{2+}/Mg^{2+} for 2 days. Crystals were harvested in 15% PEG 8000, 0.2M ammonium sulfate, 0.1M Tris-HCl, pH 8.9 plus 1mM Ca^{2+}/Mg^{2+} with glycerol as a cryoprotectant in 5% increments up to a 20% final concentration, and then flash-frozen in liquid nitrogen. We also soaked crystals with 200μM quinine in 15% PEG 8000, 0.2M ammonium sulfate, 0.1M Tris-HCl, pH 8.9, with 1mM Ca^{2+}, 5mM Mg^{2+}, and 20% glycerol for 3 days before freezing in liquid nitrogen. Because no electron density of quinine was observed, the crystal was considered a native crystal at a higher Mg^{2+} concentration. Diffraction data collected at ID-23 of APS was solved using molecular replacement. Final refinement with REFMAC5 used translation, libration, screw motion as well as noncrystallographic symmetry.

Gel filtration

The chymotrypsin-treated and purified $\alpha_{IIb}\beta_3$ headpiece at 5.6μM was incubated with RUC-1, eptifibatide, or tirofiban at 600 μM, 120μM, and 56μM, respectively, at 25°C for 1 hour and analyzed by chromatography (Superdex 200; GE Healthcare Life Sciences) in Tris-buffered saline with 1mM Ca^{2+}/Mg^{2+}.

Dynamic light scattering

Stokes radii of the chymotrypsin-treated and purified $\alpha_{IIb}\beta_3$ headpiece alone at 22μM or after mixing with RUC-1, eptifibatide, or tirofiban at 500μM, 240μM, and 56μM, respectively, were measured at 25°C by Viscotek 802 DLS (Viscotek Corporation) in Tris-buffered saline with 1mM Ca^{2+}/Mg^{2+}.

Standard MD and metadynamic simulations

MD simulations of RUC-1 alone in a water environment or bound to normal human $\alpha_{IIb}\beta_3$ were carried out using Amber 10 suite of programs (http://ambermd.org), as described in the supplemental data (available on the *Blood* Web site; see the Supplemental Materials link at the top of the online article). The well-tempered metadynamics algorithm[37-39] was used to enhance conformational sampling of RUC-1 in the binding pockets of normal or mutant human $\alpha_{IIb}\beta_3$.

RUC-1 inhibition of fibrinogen binding to normal human $\alpha_{IIb}\beta_3$ and α_{IIb} Y190F and D232H mutants

Human full-length α_{IIb} Y190F and D232H mutant cDNAs were generated by site-directed mutagenesis (QuickChange XL Site-Directed Mutagenesis Kit; Stratagene). HEK 293 transfectants were selected in 800 μg/mL G418.

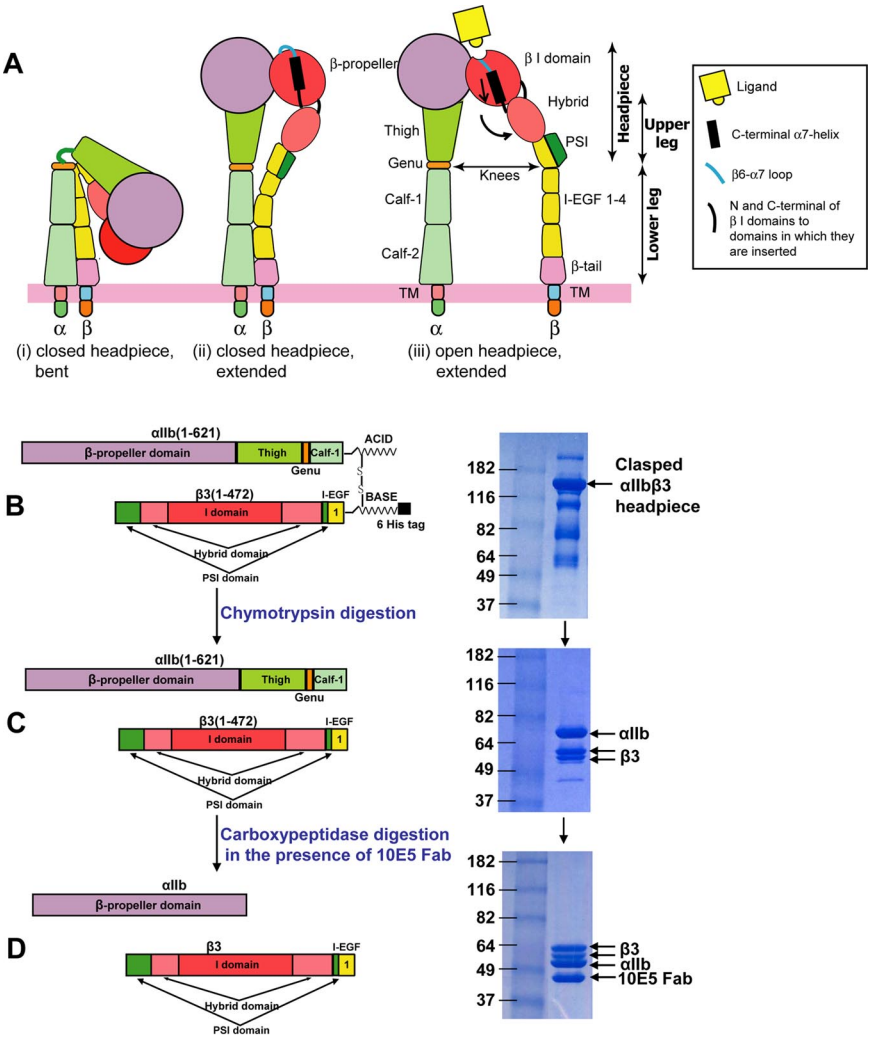

Figure 1. Cartoon models of integrin receptor conformational states and headpiece construct. (A) Three major conformational states of integrin receptor. (B-D) Integrin $\alpha_{IIb}\beta_3$ headpiece construct, protein purification, and protease digestion. The $\alpha_{IIb}\beta_3$ headpiece was first purified by Ni-NTA (B), then treated with chymotrypsin and further purified by Ni-NTA and gel filtration (C). It was then treated with carboxypeptidase in the presence of monoclonal antibody 10E5 Fab and finally purified by gel filtration (D). Protein molecular weight markers are in kDa.

The cells expressing high levels of $\alpha_{IIb}\beta_3$ were sorted based on binding of Alexa 488-conjugated monoclonal antibody (mAb) 10E5[40] (BD FACSCalibur; BD Biosciences) and expression of $\alpha_{IIb}\beta_3$ was assessed by the binding of the same antibody on each day of experimentation.

For the Alexa 488-fibrinogen binding assay, HEK293 cells were incubated in HEPES buffer-modified Tyrode solution with or without 15 μg/mL activating antibody PT25-2[41] for 5 minutes at 25°C and then Alexa 488 fibrinogen (200 μg/mL; Invitrogen) was added and incubated at 37°C for 30 minutes. Samples were then washed once and resuspended in 0.5 mL of HEPES-buffered modified Tyrode solution containing Ca^{2+}/Mg^{2+} and analyzed by flow cytometry. Net normalized fluorescence intensity (NNFI) was calculated from the geometric mean fluorescence intensity of the cells after subtracting background fluorescence and dividing by the $\alpha_{IIb}\beta_3$ receptor expression level determined by the binding of mAb 10E5. The IC_{50} of RUC-1 inhibition of fibrinogen binding to normal or mutant $\alpha_{IIb}\beta_3$ was determined after log transformation and removal of outlier values. Each NNFI value was divided by the NNFI of the PT25-2–activated sample in the absence of RUC-1. The latter sample and the maximally inhibited sample in the presence of the blocking mAb 10E5 were used to define the range of RUC-1 concentrations (0 and infinity). Mean (SD) was computed at each concentration level for normal $\alpha_{IIb}\beta_3$, α_{IIb} Y190F mutant and α_{IIb} D232H mutant. For the data with each receptor, a sigmoidal model was fitted on mean (SD) with log transformation on RUC-1 concentration to estimate the IC_{50} for fibrinogen binding (BioDataFit 1.02; Chang Bioscience Inc).

Results

Structure of a headpiece fragment in the closed conformation

Soluble headpiece protein was purified by Ni-NTA–affinity chromatography (Figure 1B right panel) and treated with chymotrypsin to remove C-terminal tags (Figure 1C). The untagged protein was digested by carboxypeptidases A and B in the presence of mAb 10E5 Fab and finally purified by gel filtration (Figure 1D). Carboxypeptidase, together with trace amounts of chymotrypsin (data not shown), removes the α_{IIb} thigh domain (note the change in α_{IIb} size in sodium dodecyl sulfate–polyacrylamide gel electrophoresis between Figure 1C-D).

The purified headpiece/Fab complex in Tris-buffered saline containing 1mM Mg^{2+} and 1mM Ca^{2+} was crystallized in 11% PEG 8000, 0.2M ammonium sulfate, and 0.1M Tris-HCl, pH 8.9 at 4°C, which gave the 2.3 Å resolution structure (native-1; Table 1). Crystals were also soaked in 5mM Mg^{2+} and 1mM Ca^{2+}, which gave the 2.25 Å resolution structure (native-2; Table 1). Both structures were refined to an R_{free} of 21.3% (Table 1). Two independent $\alpha_{IIb}\beta_3$ headpiece/Fab complexes were present per asymmetric unit (Table 1).

Table 1. Statistics of X-ray diffraction data and structure refinement

Protein	$\alpha_{IIb}\beta_3$ headpiece native-1 (1mM Mg^{2+})	$\alpha_{IIb}\beta_3$ headpiece native-2 (5mM Mg^{2+})	$\alpha_{IIb}\beta_3$ headpiece with RUC-1 (1mM Mg^{2+})
Space group	$P2_12_12$	$P2_12_12$	$P2_12_12$
Unit cell (a, b, c), Å	259.0, 144.5, 104.2	260.7, 145.2, 104.4	259.5, 144.3, 104.4
α, β, γ, °	90, 90, 90	90, 90, 90	90, 90, 90
Wavelength, Å	1.00695	0.97948	1.00795
Resolution, Å	50-2.3/2.36-2.30¶	50-2.25/2.37-2.25¶	50-2.4/2.46-2.40¶
No. of reflections, total/unique	948 770/169 848	1 244 812/187 671	807 082/145 845
Completeness, %	97.7/96.9¶	99.9/99.9¶	95.1/95.6¶
$I/\sigma(I)$	11.7/2.1¶	12.1/1.9¶	13.3/2.3¶
R_{merge}, %*	10.0/83.9¶	9.4/99.4¶	8.9/99.1¶
R_{work}†/R_{free}‡	0.177/0.213	0.172/0.213	0.172/0.216
RMSD: Bond, Å	0.007	0.009	0.007
RMSD: Angle, °	1.08	1.15	1.09
Ramachandran plot§	97.0%/2.9%/0.1%	95.3%/4.4%/0.3%	95.8%/4.0%/0.2%
Molecules/asymmetric unit	2	2	2
Resides, α_{IIb}/β_3	1-454(453)/1-466(471)**	1-457(453)/1-466(471)**	1-454(453)/1-466(467)**
Non-H atoms, protein/carbohydrate/water	20770/238/1061	20776/180/1227	20764/193/792
Protein Data Bank code	3NID	3NIG	3NIF

*$R_{merge} = \Sigma_h\Sigma_i|I_i(h) - <I(h)>|/\Sigma_h\Sigma_i|I_i(h)|$, where $I_i(h)$ and $<I(h)>$ are the ith and mean measurement of the intensity of reflection h.
†$R_{work} = \Sigma_h||F_{obs}(h)| - |F_{calc}(h)||/\Sigma_h|F_{obs}(h)|$, where $F_{obs}(h)$ and $F_{calc}(h)$ are the observed and calculated structure factors, respectively. No I/σ cutoff was applied.
‡R_{free} is the R value obtained for a test set of reflections consisting of a randomly selected 0.6% subset of data excluded from refinement.
§Residues in favorable, allowed, and outlier of the Ramachandran plot as reported by MOLPROBITY.[45]
¶Numbers correspond to the last resolution shell.
**Numbers in parentheses correspond to chains C and D.

The structures contain the α_{IIb} β-propeller domain, the β_3 plexin/semaphorin/integrin (PSI), hybrid, βI, and I-EGF1 domains, and the 10E5 Fab bound to the β-propeller cap subdomain (Figure 2A). Our previous crystal structures of the $\alpha_{IIb}\beta_3$ headpiece were obtained with a similar protein preparation in complex with ligand-mimetics or a pseudoligand, with or without 10E5 Fab.[10,11] Four molecules in unique lattice environments, 3 per asymmetric unit in the absence of Fab, and one per asymmetric unit in the presence of Fab, all adopted similar open headpiece conformations (Figure 2B). In our current headpiece structures, density for a pseudoligand was not found around the ligand-binding site; only waters surround the MIDAS Mg^{2+} (Figure 2D). The conformations of the β-propeller and the 10E5 Fab are essentially identical to those in the previous structures (Figure 2B). However, in contrast to the open conformation adopted by the liganded headpiece fragments, the unliganded $\alpha_{IIb}\beta_3$ headpiece fragments adopt the closed conformation (Figure 2B). The orientation between the βI and hybrid domains is acute, as seen in bent ectodomain structure rather than obtuse, as seen in liganded, open headpiece structures (Figure 2B).

In our closed headpiece structures, the conformation of the βI domain, including the metal ion binding sites, the β1-α1 loop, the α1-helix, the β6-α7 loop and the α7-helix, is essentially identical to the conformation seen in the bent ectodomain structures (Figure 2C). Very clear densities are seen for the Ca^{2+} in the SyMBS, the Mg^{2+} in the MIDAS, the Ca^{2+} at the ADMIDAS, and their coordinating waters in the native-2 structure in 5mM Mg^{2+} and 1 mM Ca^{2+} (Figure 2D). Similar results were obtained in the native-1 structure in 1mM Mg^{2+} and 1mM Ca^{2+}, except the densities for the MIDAS Mg^{2+} and its coordinating waters are poorly defined.

Some variation in βI/hybrid domain orientation is seen among $\alpha_{IIb}\beta_3$ and $\alpha_V\beta_3$ structures with closed headpieces, and among structures with open headpieces (Table 2). The angle between the βI and hybrid domains was ~ 12° wider in closed headpiece structures than in bent ectodomain structures (Table 2). This result was because of slight libration of the last C-terminal turn (Gly-349-Ser-353) of the α7-helix and its connecting loop to the β-strand of the hybrid domain (Figure 2C). The last turn of α-helices hydrogen bond only to preceding, and not succeeding, α-helical residues. Within the last turn of the α7-helix, beginning with Gly-349, small variations in the hydrogen bond pattern within this helical turn, and the subsequent loop permit slight rocking at the βI/hybrid interface. Similar variations (~ 12°) in βI/hybrid domain orientation were observed among the open headpiece structures in different crystal forms (Table 2), and these also correlated with libration of the last turn of the α7-helix and the following loop to the β hybrid domain. This variation is much less than that between the open and closed headpiece (Figure 2B and Table 2).

The slightly swung-out position of the hybrid domain in the closed headpiece fragment structure with respect to that in the entire ectodomain structure was associated with some remodeling of the hydrogen-bonding network at the β_3 β I/hybrid domain interface (Figure 2E-F). In particular, the hydrogen bonds between the Ser-300, Arg-360, and Asp-358 side chains, and between the Lys-417 and Asn-303 side chains, were broken (Figure 2E-F). The Arg-352 side chain, which is central in the interface, adopted a different orientation, forming new hydrogen bonds with side-chain oxygens of Tyr-348 and Gln-106 (Figure 2E-F). In addition, the Lys-422 side chain formed a hydrogen bond with the Asp-241 side chain. The hydrogen bonds between the Asp-109 side chain and the Ser-147 side chain and backbone, and between the Ser-353 backbone oxygen and the Gly-388 and Leu-389 backbone nitrogens, were maintained (Figure 2E-F). The positions of Tyr-348 and Tyr-110, which are central in the interface, were not changed (Figure 2E-F).

RUC-1 binds only to the α_{IIb} portion of the ligand binding pocket

A crystal soaked with RUC-1 diffracted to 2.4 Å (Table 1) with clear density for RUC-1 in each of the 2 molecules of the asymmetric unit (Figure 3A-B). RUC-1 binds exclusively to the

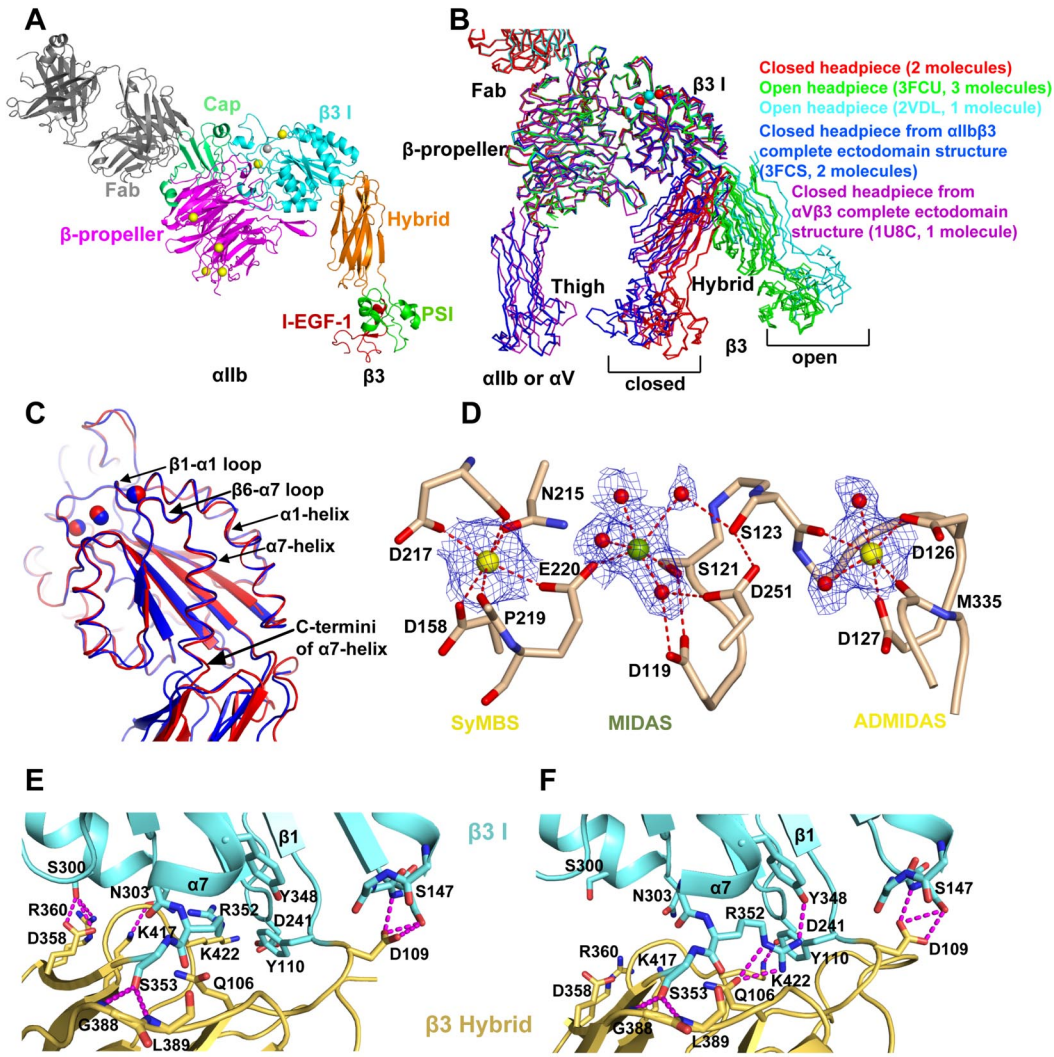

Figure 2. The crystal structure of $\alpha_{IIb}\beta_3$ headpiece in closed conformation. (A) Cartoon diagram of the $\alpha_{IIb}\beta_3$ headpiece complex with 10E5 Fab. Ca^{2+} and Mg^{2+} ions are yellow and silver spheres, respectively. (B) Superposition of the closed headpiece structure found in this study (2 molecules in one asymmetric unit, red) with the indicated previously reported structures (number of molecules per asymmetric unit). The structures were aligned on the α_{IIb}β-propeller and the β_3 βI domains by the super command of Pymol. (C) Superposition of β_3 βI domains of the closed $\alpha_{IIb}\beta_3$ headpiece structure in this study (red) and the closed headpiece structure of $\alpha_{IIb}\beta_3$ entire ectodomain (blue). Metal ions are shown as spheres. (D) 2Fo-Fc maps of metals and coordinating waters in β_3 βI domain in the presence of 5mM Mg^{2+} and 1mM Ca^{2+}. The maps are contoured at 1.5 σ. Ca^{2+} (gold) and Mg^{2+} (green) ions are large spheres. Waters (red) are small spheres. Nitrogen atoms are blue and oxygen atoms are red. Metal coordination and hydrogen bonds are dashed. (E) The β_3 βI/Hybrid interface in the complete $\alpha_{IIb}\beta_3$ ectodomain structure. (F) The β_3 βI/Hybrid interface in the closed headpiece structure. The 2 structures were aligned on the β_3 βI domain.

ligand-binding pocket formed by the α_{IIb}β-propeller domain (Figure 3A-B). In sharp contrast, the RGD-mimetic drug, tirofiban, binds to both the α_{IIb} β-propeller and β_3 βI domain[10,11] (Figure 3C). Compared with the native structure, RUC-1 did not induce any local conformational changes, such as in the β1-α1 and β6-α7 loops or α7-helix (supplemental Figure 1A).

RUC-1 fits into a hydrophobic pocket lined by α_{IIb} residues Phe-160, Tyr-190, Leu-192, and Phe-231 (Figure 3D). In the largest

Table 2. Degree of variation in β3 βI-hybrid domain orientation among β_3 integrin structures

	$\alpha_{IIb}\beta_3$ closed headpiece*	$\alpha_{IIb}\beta_3$ ectodomain (3FCS)*	$\alpha_V\beta_3$ ectodomain (3IJE)†	$\alpha_V\beta_3$ liganded ectodomain (1L5G)†	$\alpha_{IIb}\beta_3$ open headpiece‡
$\alpha_{IIb}\beta_3$ closed headpiece*	3.0°	12.6°-13.3°	11.5°-13.5°	13.9°-15.9°	51.3°-62.3°
$\alpha_{IIb}\beta_3$ ectodomain (3FCS)*	—	0.2°	7.4°-7.4°	8.2°-8.3°	57.9°-69.7°
αVβ3 ectodomain (3IJE)†	—	—	—	1.9°	55.1°-66.3°
αVβ3 liganded ectodomain (1L5G)†	—	—	—	—	55.5°-66.6°
$\alpha_{IIb}\beta_3$ open headpiece‡	—	—	—	—	1.2°-12.3°

Each pair of domains from 2 molecules was superposed using the β3 βI domain, and the change in angle upon superimposing the β3 hybrid domain was calculated.
— indicates duplicates or no comparison possible because only one structure is available.
*Two molecules in current $\alpha_{IIb}\beta_3$ closed headpiece structure and 2 molecules in Protein Data Bank (PDB) code 3FCS.
†One molecule in Protein Data Bank 3IJE and one molecule in PDB 1L5G.
‡One molecule in Protein Data Bank 2VDR and three molecules in PDB 3FCU.

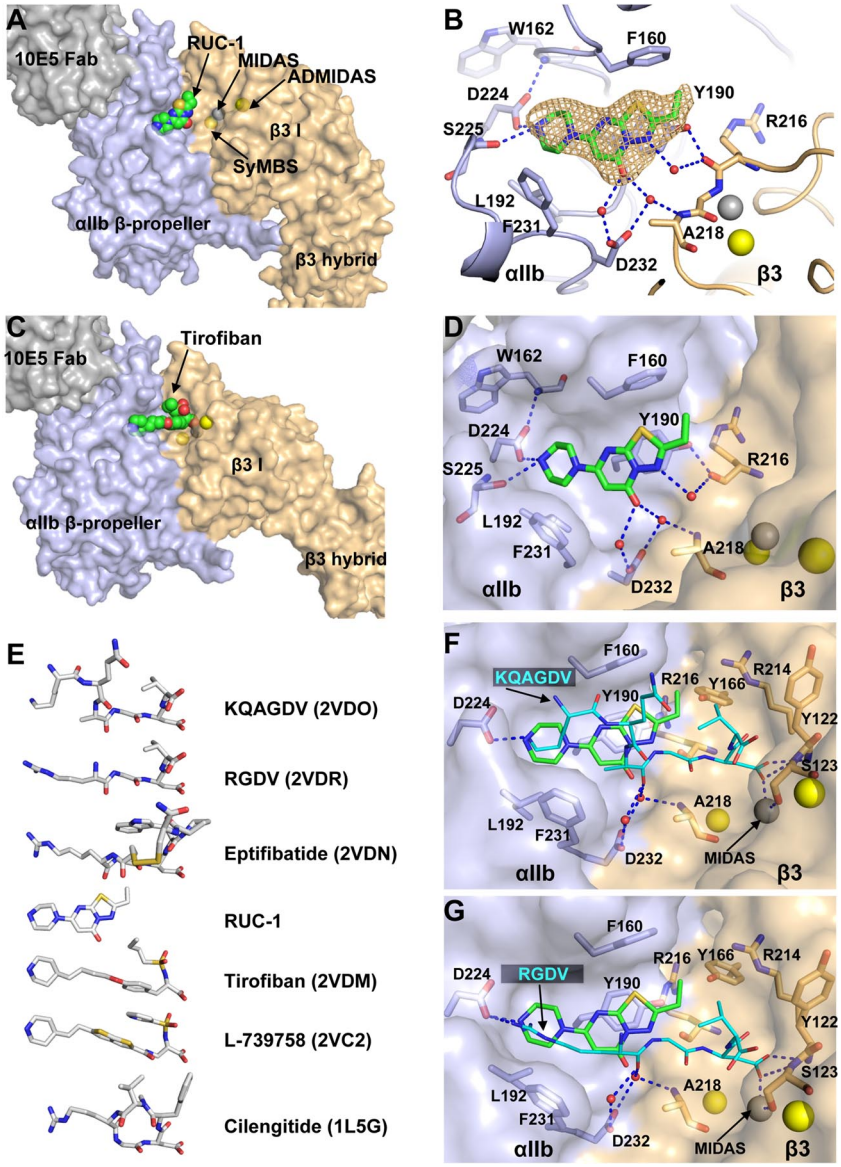

Figure 3. The binding pocket of RUC-1 in the closed $\alpha_{IIb}\beta_3$ headpiece crystal structure. (A) Overview of RUC-1 binding site. α_{IIb} (light blue), β_3 (wheat), and Fab (gray) are shown as solvent-accessible surfaces. RUC-1 is shown as spheres with green carbons, red oxygens, blue nitrogens, and yellow sulfurs. (B) Close-up of the RUC-1 binding site. Selected side chain and backbone atoms are shown in stick with other regions in cartoon. Color code is as in panel A. A simulated annealing omit map for RUC-1 is shown at 1σ. Water molecules are small red spheres. (C) The tirofiban binding site (Protein Data Bank code 2VDM). Color code is same as in panel A. Ca^{2+} ions of the SyMBS or the ADMIDAS (yellow), and the Mg^{2+} ion of MIDAS (silver) are shown as spheres. (D, F, and G) Comparison of RUC-1, KQAGDV, and RGDV binding sites. Color codes are as above, except KQAGDV and RGDV are shown as sticks with cyan carbons, after superposition on the RUC-1 complex using super command in Pymol with the α_{IIb} β-propeller and β_3 βI domains. (E) Comparison of small molecule binding locations. Crystal structures (Protein Data Bank code in parentheses) containing the indicated small molecules were superimposed as above. The ligands from the structures are shown in exactly the same alignment, except for vertical separation on the page.

hydrophobic contact, the fused ring of RUC-1 lies flat against the aromatic ring of Tyr-190 to form a π-π stacking interaction (Figure 3D). The orientation of the Tyr-190 side chain is stabilized by a hydrogen bond between the Tyr-190 hydroxyl group and the backbone carbonyl oxygen of β_3 Arg-216 (Figure 3D). The basic piperazinyl nitrogen of RUC-1 forms hydrogen bonds to the α_{IIb} Asp-224 side chain and to the backbone carbonyl oxygen of Ser-225 (Figure 3D). The side chain orientation of Asp-224 is also stabilized by a hydrogen bond with the backbone nitrogen of Trp-162 (Figure 3D). The carbonyl oxygen of RUC-1 forms hydrogen bonds to 2 water molecules that are held in place by the side chain oxygens of α_{IIb} Asp-232 (Figure 3D). RUC-1 does not have direct contact with β_3 residues. However, one of the waters that interacts with the carbonyl oxygen of RUC-1 hydrogen bonds with the β_3 Ala-218 backbone nitrogen, and one of the nitrogens of RUC-1's fused ring forms a hydrogen bond with a water molecule that is stabilized by hydrogen bonding with the carbonyl oxygen of β_3 Arg-216 (Figure 3D).

Similar to RGD-based anti-$\alpha_{IIb}\beta_3$ and anti-$\alpha_V\beta_3$ drugs, RUC-1 has a basic piperazinyl group that mimics the Lys or Arg. However, it lacks a carboxyl group mimic of the Asp (Figure 3E). RUC-1 binds to the same pocket as occupied by the Lys-Gln-Ala (KQA) sequence in the fibrinogen γC peptide KQAGDV (Figure 3F) and by the Arg of the RGD motif (Figure 3G). RUC-1 mimics the Lys or Arg by forming a hydrogen bond with Asp-224. The KQAGD sequence and RGD sequence take "upper" and "lower" paths in a hydrophobic pocket to Asp-224. It is of interest that the 3 rings of RUC-1 occupy both of these routes—and the space in between—to fill the hydrophobic binding pocket (Figure 3F-G). In addition, the RUC-1 carbonyl group mimics the water-mediated hydrogen-bond interaction of the carbonyl oxygen of the Ala of KQAGDV and the Arg of RGDV (Figure 3F-G). Compared with these peptides, RUC-1 is expected lose less entropy on binding because of its fused ring structure.

The binding pose of RUC-1 in $\alpha_{IIb}\beta_3$ headpiece crystals was almost identical to that obtained in MD simulation (Figure 4A). Several important interactions were maintained during the entire simulation, including: (1) the hydrogen bond between either of the 2 oxygens of the α_{IIb} Asp-224 carboxyl side chain and the piperazinyl nitrogen of RUC-1 (Figure 4B), (2) the hydrogen bond

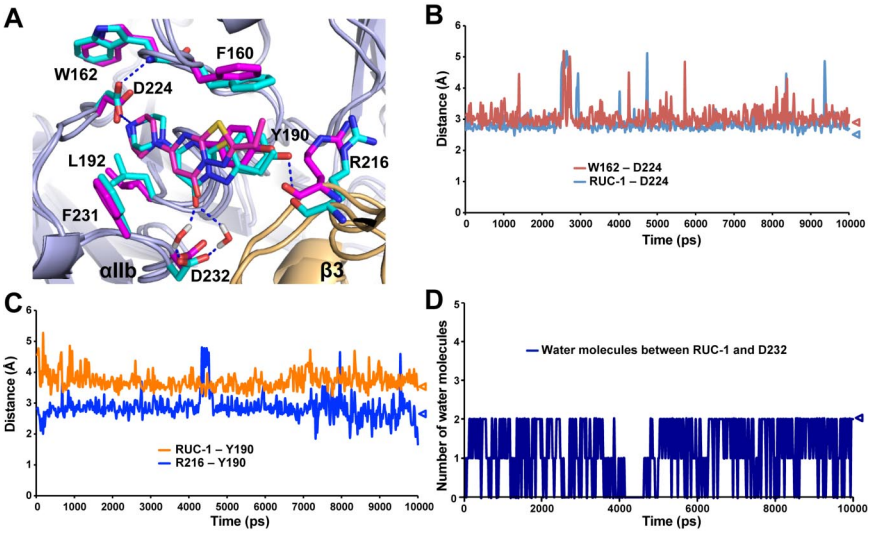

Figure 4. The binding pocket of RUC-1 studied by molecular dynamics (MD) simulations. (A) Comparison of the binding site of RUC-1 in crystal structure (magenta) and in a representative conformation (at 8 nanoseconds) of the last 5 nanoseconds of a 10-nanosecond MD simulation (cyan). The structures were aligned on the α_{IIb} β-propeller domain by Pymol. α_{IIb} and β_3 subunits are shown in light blue and wheat, respectively. (B-D) Specific distance changes during 10-nanosecond MD simulations. Values for crystal structure are indicated by triangles. (B) Minimum distance between the basic nitrogen of RUC-1 and either of the 2 oxygens of the Asp-224 side chain (blue line). Minimum distance between either of the 2 oxygens of the Asp-224 side chain and the backbone nitrogen of Trp-162 (red line). (C) Distance between the oxygen of the Tyr-190 side chain and the backbone carbonyl oxygen of β_3 Arg-216 (blue line). Distance between the centroid of the aromatic ring of Tyr-190 side chain and the centroid of the RUC-1 fused ring (orange line). (D) Number of water molecules either forming direct interactions with the RUC-1 carbonyl oxygen or interacting with the carboxyl oxygens of the Asp-232 side chain.

between the other α_{IIb} Asp-224 side chain oxygen not engaging the piperazinyl nitrogen and the backbone nitrogen of α_{IIb} Trp-162 (Figure 4B), (3) the π-π stacking interaction between the RUC-1 fused ring and the α_{IIb} Tyr-190 (Figure 4C), (4) the polar interaction between the Tyr-190 hydroxyl group and the backbone carbonyl oxygen of the β_3 Arg-216 (Figure 4C), and (5) the water molecule-mediated polar interactions between Asp-232 and the carbonyl oxygen of RUC-1 (Figure 4D).

RUC-1 specifically recognizes the human α_{IIb} integrin subunit

RUC-1 is a less potent inhibitor of mouse and rat $\alpha_{IIb}\beta_3$ and does not inhibit $\alpha_V\beta_3$.[35,36] There is no equivalent of residues Asp-224, Phe-160, and Phe-231 in α_V, consistent with lack of anti-α_V integrin activity. Human, murine, and rat α_{IIb} all have the Asp-224 that interacts with the basic piperazinyl nitrogen of RUC-1 as well as Phe-160 and Phe-231 that interact with the heterocyclic fused-ring structure of RUC-1 (Figure 3D). However, both mouse and rat have α_{IIb} Y190F substitutions. In addition, rat α_{IIb} has a D232H substitution. The Y190F substitution may change this residue's orientation because of the loss of the hydrogen bond to β_3 Arg-216, with the D232H substitution disrupting the water-mediated interaction between RUC-1 and α_{IIb} Asp-232 (Figure 3D).

Well-tempered metadynamic simulations[37] using a restraining potential to limit exploration of ligand phase space showed that RUC-1 formed the same type of interactions with the receptor as found by standard MD simulations and X-ray crystallography (supplemental Figure 2A). In contrast, this RUC-1–preferred binding mode did not correspond to the lowest-energy minima in simulations of the Y190F (supplemental Figure 2B) or D232H mutants (supplemental Figure 2C).

To test the importance of α_{IIb} Tyr-190 and Asp-232 for RUC-1 binding, we expressed Y190F and D232H mutants in HEK 293 cells. Fibrinogen bound equally well to human $\alpha_{IIb}\beta_3$ and both mutants in the presence of the activating mAb PT25-2 (Figure 5). RUC-1 blocked fibrinogen binding to HEK293 cells expressing normal human $\alpha_{IIb}\beta_3$ with an IC_{50} of 8μM (95% confidence interval [CI] 6-12μM; Figure 5). In sharp contrast, the RUC-1 IC_{50} was increased to 80μM (95% CI 45-138μM) for the α_{IIb} Y190F mutant and 1000μM (95% CI 886-1127μM) for the α_{IIb} D232H mutant.

RUC-1 does not induce conformational rearrangement of integrin $\alpha_{IIb}\beta_3$

RUC-1, unlike tirofiban and eptifibatide, does not induce conformational changes in β_3, as judged by the binding of the β_3 LIBS mAb AP5. Nor does it induce ligand binding, as judged by a priming assay.[35] The crystal structure data in the current study showed that RUC-1 failed to initiate movements in the β1-α1 and β6-α7 loops or the α7-helix. However, since lattice contacts could interfere with large structural rearrangements, such as hybrid domain swing out, we examined the effect of RUC-1 on the conformation of the $\alpha_{IIb}\beta_3$ headpiece in solution.

Induction of conformational change in $\alpha_{IIb}\beta_3$ was measured by an increase in Stokes radius in gel filtration or DLS. In these experiments, the chymotrypsin-treated, purified $\alpha_{IIb}\beta_3$ headpiece, including the α_{IIb} thigh domain (see "Methods" and Figure 1C) was analyzed before and after mixing with saturating concentrations of RUC-1, tirofiban, or eptifibatide. RUC-1 did not induce a shift in the elution volume of the $\alpha_{IIb}\beta_3$ headpiece in gel filtration (Figure 6A). In contrast, tirofiban and eptifibatide each substantially shifted elution volume, indicating a less compact structure (Figure 6A-B).

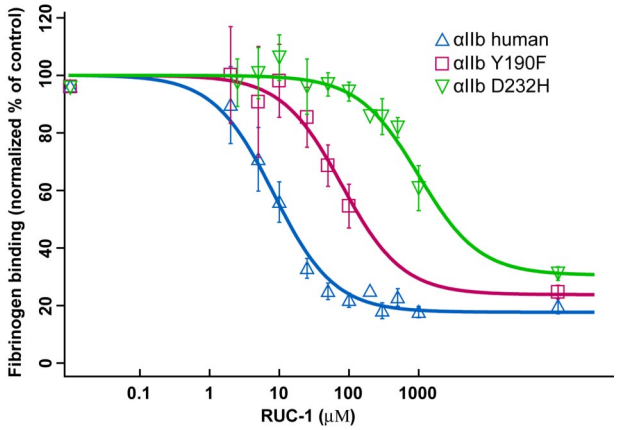

Figure 5. The α_{IIb} Y190F and D232H mutations increase the RUC-1 IC_{50} for fibrinogen. Fibrinogen binding to cells expressing normal human $\alpha_{IIb}\beta_3$, the α_{IIb} Y190F mutant, or the α_{IIb} D232H mutant receptor in the presence of the activating monoclonal antibody PT25-2 was determined. The data were normalized and the mean ± standard error of the mean (SEM) for each concentration of RUC-1 tested is depicted.

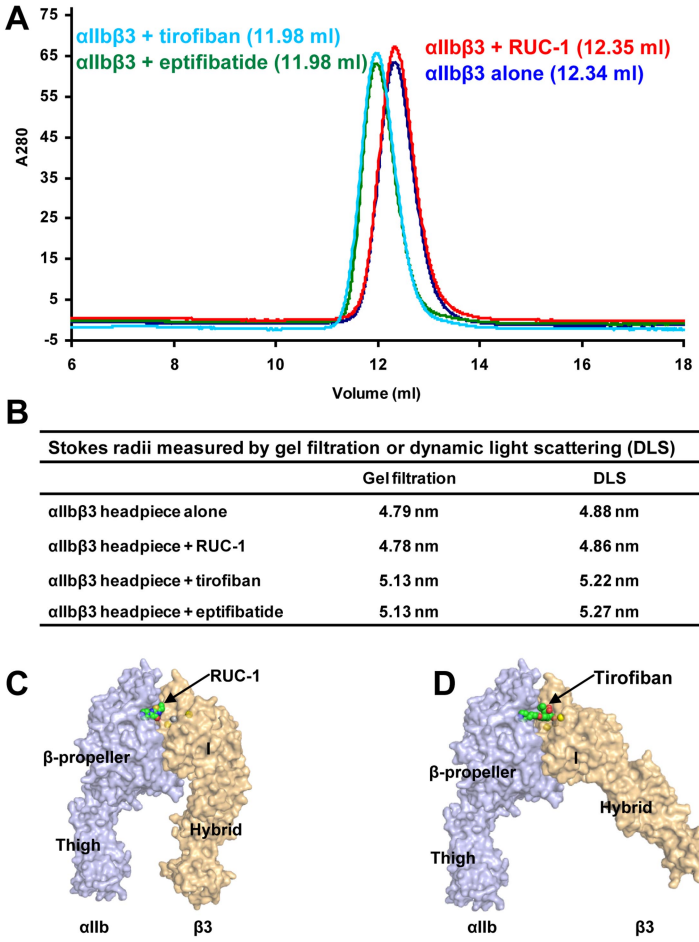

Figure 6. Conformational change of integrin $\alpha_{IIb}\beta_3$ headpiece studied by gel filtration and dynamic light scattering. (A) Gel filtration profile of $\alpha_{IIb}\beta_3$ headpiece alone or bound with antagonists. The untagged $\alpha_{IIb}\beta_3$ headpiece was mixed with saturating amounts of RUC-1, tirofiban, or eptifibatide and incubated at room temperature for 1 hour before Superdex 200 chromatography in Tris-buffered saline with 1mM Ca^{2+}/Mg^{2+}. The elution volumes are shown in parentheses. (B) Stokes radius measured by gel filtration or dynamic light scattering. (C-D) The structures with surface representation indicate the putative conformational rearrangement after drug binding. The structures were generated by adding the α_{IIb} thigh domain from the complete ectodomain structure to the headpiece crystal structures. The Ca^{2+} and Mg^{2+} ions are shown as yellow and silver spheres, respectively. RUC-1 (C) and tirofiban (D) are shown as spheres.

B

Stokes radii measured by gel filtration or dynamic light scattering (DLS)		
	Gel filtration	DLS
αIIbβ3 headpiece alone	4.79 nm	4.88 nm
αIIbβ3 headpiece + RUC-1	4.78 nm	4.86 nm
αIIbβ3 headpiece + tirofiban	5.13 nm	5.22 nm
αIIbβ3 headpiece + eptifibatide	5.13 nm	5.27 nm

When measured by DLS, the Stokes radii for the $\alpha_{IIb}\beta_3$ headpiece were 4.88 nm and 4.86 nm in the absence and presence of RUC-1, respectively (Figure 6B)—a result that is again consistent with the absence of a conformational rearrangement (Figure 6C). In contrast, tirofiban and eptifibatide both increased the Stokes radius of the $\alpha_{IIb}\beta_3$ headpiece, to 5.27 nm and 5.22 nm, respectively (Figure 6B)—corresponding with what would be expected from a swing-out motion of the β_3 hybrid domain (Figure 6D). Estimates of the Stokes radii with HYDROPRO[42] were 4.68 nm for the closed headpiece structure (Figure 6C) and 5.03 nm for the open headpiece structure (Figure 6D). The Stokes radii measurements demonstrate that the $\alpha_{IIb}\beta_3$ headpiece in solution remains in a compact closed conformation after treatment with RUC-1.

Discussion

In our integrin $\alpha_{IIb}\beta_3$ headpiece fragment preparation, the α_{IIb} subunit was truncated after the β-propeller domain; the β_3 subunit was truncated after the I-EGF1 domain (Figure 1D). Before this work, all crystal structures showing the closed headpiece were of intact ectodomains in the bent conformation,[3-5] whereas all crystal structures showing the open headpiece were of the same headpiece fragment used here.[10] Open headpiece crystal structures have been obtained with or without 10E5 Fab, which binds a region of α_{IIb} with our current closed headpiece crystal structure, that does not shift in allostery.[11] Together with our current closed headpiece crystal structure, these data exclude the possibility that leg truncation alone is sufficient to induce hybrid domain swing out.[12]

The presence of closed and open integrin headpieces in crystal structures, in the absence of constraints imposed by contacts with the lower legs, is a finding that is in agreement with EM studies of integrins $\alpha_V\beta_3$, $\alpha_L\beta_2$, and $\alpha_X\beta_2$—all of which revealed closed and open headpiece conformations in extended integrins, with the closed headpiece conformation predominating under nonactivating conditions.[15,17,43] EM study of the $\alpha_5\beta_1$ headpiece also revealed a closed conformation in the absence of ligand.[16] Cocrystals of the $\alpha_{IIb}\beta_3$ headpiece with 3 ligand-mimetic antagonists all demonstrated the open conformation.[11] It is of interest that the cacodylate ion was found to act as a pseudo-ligand, coordinating the β_3 MIDAS and stabilizing the open conformation when the $\alpha_{IIb}\beta_3$ headpiece was crystallized in the absence of antagonists.[11] No electron density for such a pseudo-ligand was found in the closed headpiece crystal structure in the current study. Instead, we observed ordered water molecules around the MIDAS Mg^{2+} ion. Similarly, none of the closed headpiece, bent ectodomain crystal structures showed an electron density corresponding to a ligand or pseudo-ligand. We conclude that the presence of a closed or open headpiece correlates with the absence or presence of MIDAS ligation, respectively, and does not correlate with the absence or presence of leg domains. In vivo, two mechanisms are thought to stabilize the high affinity, open headpiece conformation. One is binding to ligand. The other is lateral force exerted parallel to the direction of hybrid domain swing out by actin cytoskeleton association with the integrin β-subunit cytoplasmic domain.[5]

The two independent $\alpha_{IIb}\beta_3$ headpiece molecules in our crystal asymmetric unit provide further information on the range of βI/hybrid domain orientations and interfaces accessible in the

closed headpiece conformation. The conformation of the βI domain in our closed headpiece structure is essentially identical with that of the bent $\alpha_{IIb}\beta_3$ entire ectodomain structure, with Cα-RMSD of 0.48 Å for residues Asp-109-Ser-353. However, the orientation between the βI/hybrid domains varied between the closed headpiece and the bent ectodomain structures. In addition, some of the hydrogen-bond networks in the βI/hybrid interface were remodeled in our closed headpiece structure (Figure 2E,F). Interestingly, similar variations in βI/hybrid domain orientation were observed among the open headpiece structures in different crystal forms (Table 2). These variations are all the result of displacement at the last turn of the α7-helix and its linked loop to the β hybrid domain.

Similar to our previous structure of the complete $\alpha_{IIb}\beta_3$ ectodomain, we found that MIDAS, SyMBS, and ADMIDAS were preloaded with metal ions when the protein solution contained 1mM Mg^{2+} and 1mM Ca^{2+}, even though the crystallization well solution did not contain cations. Metal ion occupancy of SyMBS and ADMIDAS with Ca^{2+} was complete under these conditions, whereas occupancy of MIDAS was partial. Occupancy of all sites was complete when the crystals were soaked in the well solution containing 5mM Mg^{2+} and 1mM Ca^{2+}. Furthermore, excellent densities were observed for all of the water molecules in the inner, octahedral coordination shells of MIDAS Mg^{2+} and ADMIDAS Ca^{2+}. The apparently looser binding of MIDAS Mg^{2+} compared with the ADMIDAS Ca^{2+} may be the result of its coordination by only 2 groups supplied by the protein; the other 4 inner coordinations are to water. The finding in an $\alpha_V\beta_3$ ectodomain structure that there is a lack of metal ion at the SyMBS, and only partial occupancy at MIDAS,[3,6] is explicable based on the use of only Ca^{2+} in crystallization, the synergy between Ca^{2+} and Mg^{2+} in integrin ligand binding, and the coordination of SyMBS and MIDAS by Glu-220 (Zhu et al[5] and references therein). Our results showing that metals are preloaded make the proposal highly unlikely that metal binding to SyMBS and MIDAS is induced by ligand binding.[3,23] Furthermore, MIDAS is buried by ligand binding, and SyMBS, which is completely surrounded by protein ligands, is already buried with no water accessibility before ligand binding and becomes buried more deeply afterward.

Role of binding to βI MIDAS metal ion and β1-α1 backbone in headpiece opening

Comparison of our unliganded closed $\alpha_{IIb}\beta_3$ headpiece structure with our previously described liganded open $\alpha_{IIb}\beta_3$ headpiece structure, along with the failure of RUC-1 to induce the open conformation of β_3, supports the hypothesis that engaging the MIDAS metal ion and the β1-α1 loop backbone by the ligand carboxyl group is the mechanism by which ligand binding triggers adoption of the open conformation. It could be argued that crystal contacts prevented $\alpha_{IIb}\beta_3$ from adopting the open conformation when RUC-1 was soaked into the crystal. However, soaking the RGD-based antagonist cilengitide into the $\alpha_V\beta_3$ ectodomain crystal induced the movement of the β1-α1 loop, the breaking of the Met-335 carbonyl coordination of the ADMIDAS metal ion, and ADMIDAS metal ion movement toward MIDAS[23] (supplemental Figure 1B). Moreover, soaking tirofiban or eptifibatide into our closed headpiece crystals also induced similar local conformational changes (J.Z., J.Z., T.A.S., unpublished data, 2010).

Our biophysical studies demonstrated that RUC-1 does not alter the gel filtration or DLS properties of the $\alpha_{IIb}\beta_3$ headpiece, providing support for it not inducing a conformational change in β_3. In contrast, eptifibatide and tirofiban each induced an increase in Stokes radius of approximately 0.34 nm. This increase is in accord with the calculated increase of 0.35 nm in Stokes radius using the coordinates of the closed and open headpiece structures. Thus, these results provide strong support for the hypothesis that tirofiban and eptifibatide induce hybrid domain swing out in solution. The difference between RUC-1 and the traditional RGD antagonists in their ability to induce hybrid domain swing out provides additional support for the importance of the MIDAS-coordinating carboxyl group in inducing this conformational change. Ligand engagement of the β_3 I domain, and in particular coordination to the MIDAS metal ion and hydrogen bonds to the backbone of the β1-α1 loop, is therefore the most likely trigger for β_3 swing out. These interactions may be sufficient to induce opening because the cacodylate ion, acting as an $\alpha_{IIb}\beta_3$ pseudoligand and binding exclusively to the MIDAS metal ion and the backbone of the β1-α1 loop, was associated with the open conformation.[11]

Implications for novel drug design

Previous attempts to target $\alpha_{IIb}\beta_3$ and other integrin receptors that bind RGD-containing peptides have focused on developing high-affinity congeners that mimic the RGD sequence in having both positive and negative charge groups separated by a distance similar to that in RGD peptides. The weight of evidence now suggests that such molecules may induce conformational changes that are undesirable in that they can induce the high-affinity ligand binding state of the receptor and can expose regions of the receptor that can serve as neoepitopes for preexisting or induced antibodies that may be responsible, in part, for the thrombocytopenia associated with these agents.[44] Our studies with RUC-1 indicate that it is possible to identify molecules that can block ligand binding without engaging the β_3 MIDAS metal ion or inducing either a high-affinity binding state or a major conformational change in the β_3 subunit. Moreover, RUC-1 demonstrates that it is possible to obtain high specificity for human $\alpha_{IIb}\beta_3$ relative to human $\alpha_V\beta_3$—and even $\alpha_{IIb}\beta_3$ from other species—with a small molecule that binds exclusively to α_{IIb}. Although RUC-1 has considerably lower affinity for $\alpha_{IIb}\beta_3$ than eptifibatide or tirofiban, it is within the range of affinities of a sizable percentage of drugs. Thus, RUC-1 provides important proof of concept in designing a new class of integrin receptor antagonists that may have therapeutic advantages over those based on the RGD sequence.

Acknowledgments

We thank Jihong Li of Rockefeller University for site-directed mutagenesis and fibrinogen binding studies and Tingting Song of Rockefeller University for statistical analyses.

This work was supported in part by grants from the National Institutes of Health (HL19278, HL46875, and ULRR024143) and Stony Brook University. Computational resources were obtained from NSF TeraGrid (MRAC MCB080077).

Authorship

Contribution: Jieqing Zhu, Jianghai Zhu, A.N., and D.P. performed research, analyzed data, and wrote the paper; M.F. and B.S.C. designed some of the studies, analyzed data, and wrote the

paper; T.A.S. supervised the research and data analysis and wrote the paper.

Conflict-of-interest disclosure: B.S.C. is an inventor of abciximab (Centocor) and the VerifyNow assay (Accumetrics Inc), and in accord with federal law and the policies of the Research Foundation of the State University of New York at Stony Brook and Mount Sinai School of Medicine, respectively, he shares in royalty payments. Rockefeller University has applied for a patent on RUC-1 and B.S.C. may ultimately share in royalties from RUC-1. B.S.C. serves as a consultant to Accumetrics Inc. The remaining authors declare no competing financial interests.

Correspondence: Timothy A. Springer, Immune Disease Institute, Children's Hospital Boston, and Department of Pathology, Harvard Medical School, Boston, MA 02115; e-mail: springer@idi.harvard.edu.

References

1. Springer TA, Wang J-H. The three-dimensional structure of integrins and their ligands, and conformational regulation of cell adhesion. *Adv Protein Chem.* 2004;68:29-63.
2. Hynes RO. Integrins: bi-directional, allosteric, signalling machines. *Cell.* 2002;110(6):673-687.
3. Xiong JP, Mahalingham B, Alonso JL, et al. Crystal structure of the complete integrin alphaVbeta3 ectodomain plus an alpha/beta transmembrane fragment. *J Cell Biol.* 2009;186(4):589-600.
4. Xie C, Zhu J, Chen X, et al. Structure of an integrin with an alpha I domain, complement receptor type 4. *EMBO J.* 2010;29(3):666-679.
5. Zhu J, Luo BH, Xiao T, et al. Structure of a complete integrin ectodomain in a physiologic resting state and activation and deactivation by applied forces. *Mol Cell.* 2008;32(6):849-861.
6. Xiong J-P, Stehle T, Diefenbach B, et al. Crystal structure of the extracellular segment of integrin alphaVbeta3. *Science.* 2001;294(5541):339-345.
7. Luo BH, Carman CV, Springer TA. Structural basis of integrin regulation and signaling. *Annu Rev Immunol.* 2007;25:619-647.
8. Adair BD, Xiong JP, Maddock C, et al. Three-dimensional EM structure of the ectodomain of integrin alphaVbeta3 in a complex with fibronectin. *J Cell Biol.* 2005;168(7):1109-1118.
9. Arnaout MA, Goodman SL, Xiong JP. Structure and mechanics of integrin-based cell adhesion. *Curr Opin Cell Biol.* 2007;19(5):495-507.
10. Springer TA, Zhu J, Xiao T. Structural basis for distinctive recognition of fibrinogen by the platelet integrin aIIbb3. *J Cell Biol.* 2008;182(4):791-800.
11. Xiao T, Takagi J, Wang J-H, et al. Structural basis for allostery in integrins and binding of fibrinogen-mimetic therapeutics. *Nature.* 2004;432(7013):59-67.
12. Arnaout MA, Mahalingam B, Xiong JP. Integrin structure, allostery, and bidirectional signaling. *Annu Rev Cell Dev Biol.* 2005;21:381-410.
13. Humphries MJ. Monoclonal antibodies as probes of integrin priming and activation. *Biochem Soc Trans.* 2004;32(Pt 3):407-411.
14. Mould AP, Symonds EJ, Buckley PA, et al. Structure of an integrin-ligand complex deduced from solution X-ray scattering and site-directed mutagenesis. *J Biol Chem.* 2003;278(41):39993-39999.
15. Takagi J, Petre BM, Walz T, et al. Global conformational rearrangements in integrin extracellular domains in outside-in and inside-out signaling. *Cell.* 2002;110(5):599-611.
16. Takagi J, Strokovich K, Springer TA, et al. Structure of integrin alpha5beta1 in complex with fibronectin. *EMBO J.* 2003;22(18):4607-4615.
17. Nishida N, Xie C, Shimaoka M, et al. Activation of leukocyte beta2 integrins by conversion from bent to extended conformations. *Immunity.* 2006;25(4):583-594.
18. D'Souza SE, Haas TA, Piotrowicz RS, et al. Ligand and cation binding are dual functions of a discrete segment of the integrin beta3 subunit: cation displacement is involved in ligand binding. *Cell.* 1994;79(4):659-667.
19. Coller BS, Shattil SJ. The GPIIb/IIIa (integrin alphaIIbbeta3) odyssey: a technology-driven saga of a receptor with twists, turns, and even a bend. *Blood.* 2008;112(8):3011-3025.
20. Kloczewiak M, Timmons S, Bednarek MA, et al. Platelet receptor recognition domain on the gamma chain of human fibrinogen and its synthetic peptide analogues. *Biochemistry.* 1989;28(7):2915-2919.
21. Scarborough RM, Gretler DD. Platelet glycoprotein IIb-IIIa antagonists as prototypical integrin blockers: novel parenteral and potential oral antithrombotic agents. *J Med Chem.* 2000;43(19):3453-3473.
22. Coller BS. Anti-GPIIb/IIIa drugs: current strategies and future directions. *Thromb Haemost.* 2001;86(1):427-443.
23. Xiong JP, Stehle T, Zhang R, et al. Crystal structure of the extracellular segment of integrin alphaVbeta3 in complex with an Arg-Gly-Asp ligand. *Science.* 2002;296(5565):151-155.
24. Zhu J, Boylan B, Luo B-H, et al. Tests of the extension and deadbolt models of integrin activation. *J Biol Chem.* 2007;282(16):11914-11920.
25. Alghisi GC, Ponsonnet L, Ruegg C. The integrin antagonist cilengitide activates alphaVbeta3, disrupts VE-cadherin localization at cell junctions and enhances permeability in endothelial cells. *PLoS One.* 2009;4(2):e4449.
26. Jennings LK, Haga JH, Slack SM. Differential expression of a ligand induced binding site (LIBS) by GPIIb-IIIa ligand recognition peptides and parenteral antagonists. *Thromb Haemost.* 2000;84(6):1095-1102.
27. Kouns WC, Kirchhofer D, Hadvary P, et al. Reversible conformational changes induced in glycoprotein IIb-IIIa by a potent and selective peptidomimetic inhibitor. *Blood.* 1992;80(10):2539-2547.
28. Peter K, Schwarz M, Ylanne J, et al. Induction of fibrinogen binding and platelet aggregation as a potential intrinsic property of various glycoprotein IIb/IIIa (alphaIIbbeta3) inhibitors. *Blood.* 1998;92(9):3240-3249.
29. Bassler N, Loeffler C, Mangin P, et al. A mechanistic model for paradoxical platelet activation by ligand-mimetic alphaIIbbeta3 (GPIIb/IIIa) antagonists. *Arterioscler Thromb Vasc Biol.* 2007;27(3):e9-e15.
30. Gao C, Boylan B, Bougie D, et al. Eptifibatide-induced thrombocytopenia and thrombosis in humans require FcgammaRIIa and the integrin beta3 cytoplasmic domain. *J Clin Invest.* 2009;119(3):504-511.
31. Bougie DW, Wilker PR, Wuitschick ED, et al. Acute thrombocytopenia after treatment with tirofiban or eptifibatide is associated with antibodies specific for ligand-occupied GPIIb/IIIa. *Blood.* 2002;100(6):2071-2076.
32. Epelman S, Nair D, Downey R, et al. Eptifibatide-induced thrombocytopenia and thrombosis. *J Thromb Thrombolysis.* 2006;22(2):151-154.
33. Chew DP, Bhatt DL, Sapp S, et al. Increased mortality with oral platelet glycoprotein IIb/IIIa antagonists: a meta-analysis of phase III multicenter randomized trials. *Circulation.* 2001;103(2):201-206.
34. Cox D. Oral GPIIb/IIIa antagonists: what went wrong? *Curr Pharm Des.* 2004;10(14):1587-1596.
35. Blue R, Murcia M, Karan C, et al. Application of high-throughput screening to identify a novel alphaIIb-specific small-molecule inhibitor of alphaIIbbeta3-mediated platelet interaction with fibrinogen. *Blood.* 2008;111(3):1248-1256.
36. Blue R, Kowalska MA, Hirsch J, et al. Structural and therapeutic insights from the species specificity and in vivo antithrombotic activity of a novel alphaIIb-specific alphaIIbbeta3 antagonist. *Blood.* 2009;114(1):195-201.
37. Barducci A, Bussi G, Parrinello M. Well-tempered metadynamics: a smoothly converging and tunable free-energy method. *Phys Rev Lett.* 2008;100(2):020603.
38. van der Spoel D, Lindahl E, Hess B, et al. GROMACS: fast, flexible, and free. *J Comput Chem.* 2005;26(16):1701-1718.
39. Bonomi M, Branduardi D, Bussi G, et al. PLUMED: A portable plugin for free-energy calculations with molecular dynamics. *Comp Phys Comm.* 2009;180(10):1961-1972.
40. Coller BS, Peerschke EI, Scudder LE, et al. A murine monoclonal antibody that completely blocks the binding of fibrinogen to platelets produces a thrombasthenic-like state in normal platelets and binds to glycoproteins IIb and/or IIIa. *J Clin Invest.* 1983;72(1):325-338.
41. Tokuhira M, Handa M, Kamata T, et al. A novel regulatory epitope defined by a murine monoclonal antibody to the platelet GPIIb-IIIa complex (alphaIIbbeta3 integrin). *Thromb Haemost.* 1996;76(6):1038-1046.
42. García De La Torre J, Huertas ML, Carrasco B. Calculation of hydrodynamic properties of globular proteins from their atomic-level structure. *Biophys J.* 2000;78(2):719-730.
43. Luo B-H, Springer TA. Integrin structures and conformational signaling. *Curr Opin Cell Biol.* 2006;18(5):579-586.
44. Aster RH, Bougie DW. Drug-induced immune thrombocytopenia. *N Engl J Med.* 2007;357(6):580-587.
45. Davis IW, Leaver-Fay A, Chen VB, et al. MolProbity: all-atom contacts and structure validation for proteins and nucleic acids. *Nucleic Acids Res.* 2007;35:W375-383